Science of the Total Environment 616–617 (2018) 1279–1287

Contents lists available at ScienceDirect

Science of the Total Environment

journal homepage: www.elsevier.com/locate/scitotenv

Protonation-dependent heterogeneity in fluorescent binding sites in sub-fractions of fulvic acid using principle component analysis and two-dimensional correlation spectroscopy

Fanhao Song [a], Fengchang Wu [a], Baoshan Xing [b], Tingting Li [a], Weiying Feng [a], John P. Giesy [a,c], Wenjing Guo [a], Hao Wang [a], Shasha Liu [a], Yingchen Bai [a,*]

[a] State Key Laboratory of Environmental Criteria and Risk Assessment, Chinese Research Academy of Environmental Science, Beijing 10012, China
[b] Stockbridge School of Agriculture, University of Massachusetts, Amherst, MA 01003, USA
[c] Department of Biomedical and Veterinary Biosciences and Toxicology Centre, University of Saskatchewan, Saskatoon, Saskatchewan S7N 5B3, Canada

HIGHLIGHTS

- Heterogeneous proton binding sites in FA sub-fractions were studied by fluorescence spectroscopy.
- Heterogeneity of proton binding sites was observed among fulvic/humic/protein-like materials.
- Each of fulvic/tryptophan-like materials also presented heterogeneous binding sits to proton.
- Protein-like materials had larger p*K*a (4.17–5.29) than fulvic/humic-like materials (2.20–3.38).
- Different p*K*a values of materials were agreement with sequential orders from asynchronous maps.

GRAPHICAL ABSTRACT

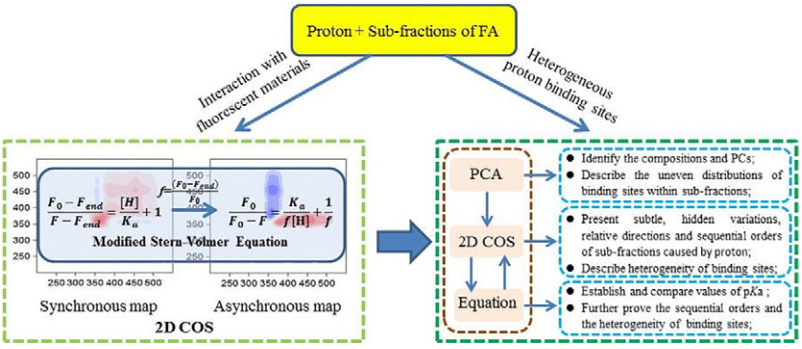

ARTICLE INFO

Article history:
Received 28 August 2017
Received in revised form 18 October 2017
Accepted 18 October 2017
Available online 21 October 2017

Editor: Jay Gan

Keywords:
Synchronous-asynchronous maps
Modified Stern-Volmer equation
Dissociation constant
Sequential variations

ABSTRACT

Heterogeneous distributions of proton binding sites within sub-fractions of fulvic acid (FA_3–FA_{13}) were investigated by use of synchronous fluorescence spectra (SFS), combined with principle component analysis (PCA) and two-dimensional correlation spectroscopy (2D-COS). Tryptophan-like, fulvic-like and humic-like materials were observed in SFS. Tyrosine-like materials were identified by use of SFS-PCA analysis. Combined information from synchronous-asynchronous maps and dissociation constants (p*K*a) was used to describe heterogeneity of binding sites for protons within each sub-fraction. Heterogeneous distributions of proton binding sites were observed in fulvic-like, humic-like, tryptophan-like, and tyrosine-like materials of five sub-fractions and even in the single fulvic-like materials in FA_3 and tryptophan-like materials in FA_9 and FA_{13}. Values of p*K*a of sub-fractions ranged from 2.20 to 5.29, depending on associated wavelengths in synchronous-asynchronous maps and use of the modified Stern-Volmer equation. The larger values of p*K*a (4.17–5.29) were established for protein-like materials (including tryptophan-like and tyrosine-like materials) in comparison to those (2.20–3.38) for humic-like and fulvic-like materials in sub-fractions. Sequential variations of 274 nm (p*K*a 4.15–5.29) → 360–460 nm (p*K*a 2.78–2.39) for FA_5–FA_{13} revealed that binding of protons to tryptophan-like materials appeared prior to humic-like/fulvic-like materials. In FA_9, protons were preferentially binding to tryptophan-like materials than tyrosine-like materials. In FA_3, protons were preferentially binding to humic-like materials than fulvic-like materials. Relative differences of values of p*K*a for fluorescent materials within each sub-fraction were consistent with

* Corresponding author.
E-mail address: baiyc@craes.org.cn (Y. Bai).

https://doi.org/10.1016/j.scitotenv.2017.10.190

sequential orders derived from asynchronous maps. Such an integrated approach, SFS-PCA/2D-COS, has superior potential for further applications in exploring complex interactions between dissolved organic matter and contaminants in engineered and natural environments.

1. Introduction

Fulvic acid (FA) is ubiquitous in aquatic and soil environments. FAs, which comprise a range of molecular structures with various proportions of functional groups, are a more mobile hydrophobic acid fraction of dissolved organic matter (DOM) (Bai et al., 2015; Berkovic et al., 2012; Lochmueller and Saavedra, 1986). FA is known to affect mobilization, bioavailability or reactivity of environmental contaminants, such as metal ions, polycyclic aromatic hydrocarbons and other chemical species (Cabaniss and Shuman, 2002; Chin et al., 2004; Gauthier et al., 1986; Giesy and Alberts, 1982; Giesy et al., 2010; Giesy and Briese, 1980; Iimura et al., 2012). In aquatic systems, protons can affect functionalities and configurations of DOM and intermolecular interactions of DOM with environmental contaminants (De Haan et al., 1983; Lu and Jaffe, 2001; Pace et al., 2012; Wu et al., 2004). For example, protons can affect binding of metal ions (e.g., Cu^{2+}, Hg^{2+}) to DOM because protons and metal ions compete for similar types of binding sites (Lu and Jaffe, 2001; Wu et al., 2004). However, due to structural heterogeneity of compositions, as well as challenging operational separations of FA (Bai et al., 2015; Hur and Lee, 2011a; Lehmann and Kleber, 2015), it is still difficult to fully understand interactions between FA and protons.

Due to abundant functional groups in natural DOM, that fluorescence spectroscopy is the most frequently used tool to investigate protonation-dependent characteristics of DOM (Geng et al., 2010; Yan et al., 2013). Synchronous fluorescence spectra (SFS) analysis can be used to distinguish the presence of fluorescent materials and establish proton or metal binding parameters based on spectral information (Cabaniss, 2002; Pullin and Cabaniss, 1995). However, due to the strong overlaps between the fluorescence peaks, resolution of structural components of DOM by use of SFS might not be satisfactory (Cabaniss, 2002; Geng et al., 2010; Pullin and Cabaniss, 1995). Investigation of overall binding behaviors of protons or metals, by use of selected peak wavelength pairs, has been criticized for violating the underlying assumption of a homogeneous distribution of proton or metal binding sites within DOM. Based on SFS data, principal component analysis (PCA) is a powerful method to identify principle components (PCs) and determine correlations and classification from fluorescence of DOM (Esteves et al., 2006; Guo et al., 2013; Sakurai and Goto, 2007; Su et al., 2016). PCA presents a further strategy for reduction of extensive spectroscopic overlap and rejection of matrix interferences (Esteves et al., 2006; Guo et al., 2013; Su et al., 2016). Slight compositional variations of DOM in leachates over hydrophobicity and polarity, as well as changes in conformation of standard humic substances at variable pH had been identified by use of SFS combined with PCA (Pullin and Cabaniss, 1995; Su et al., 2016). 2D COS is useful for simplifying complex spectra consisting of many overlapping peaks to enhance spectral resolution and identify order of subtle spectral changes in response to external perturbations (Chen et al., 2015; Hur et al., 2011; Hur and Lee, 2011a; Maqbool and Hur, 2016; Noda, 1990; Su et al., 2016). 2D COS has been utilized to present subtle, hidden variations, relative directions and sequential order of DOM caused by various factors, such as temperature, irradiation, metal ions and anionic surfactant addition (Hur and Lee, 2011a; Lü et al., 2013; Maqbool and Hur, 2016; Xu et al., 2013). To better understand their interactions and environmental behaviors, heterogeneous binding sites for metal ions (e.g., Cu^{2+}, Hg^{2+}) within DOM have been widely studied by use of 2D COS (Hur and Lee, 2011a; Hur and Lee, 2011b). Furthermore, overlapped peaks from SFS-PCA could be selected as wavelength pairs to support the analysis of spectral variations from 2D COS. However, application of SFS-PCA/2D COS to better understand possible protonation-dependent heterogeneity in fluorescent binding sites of FA has received little attention.

Fluorescence titration combined with analysis of data by use of the modified Stern-Volmer equation has been employed to describe affinities of binding of metals, such as Cu^{2+} or Hg^{2+} to DOM and organic contaminants, such as the PAH or phenanthrene (Berkovic et al., 2012; Esteves da Silva et al., 1998; Hur et al., 2011; Lu and Jaffe, 2001). Overall, conditional stability constants have been successfully used to estimate heterogeneity of binding of metal ions to DOM (Guo et al., 2012; Hays et al., 2004; Hur and Lee, 2011a, 2011b). However, the modified Stern-Volmer equation has not been used to estimate dissociation constants (p*K*a) of sub-fractions of FA by use of SFS data. By comparing values of p*K*a derived during this study, sequential orders of sub-fractions affected by pH were described by use of synchronous-asynchronous maps with 2D COS.

To reduce structural heterogeneity of FA, soil FA was separated into sub-fractions by use of XAD-8 adsorption, coupled with stepwise elution by use of pyrophosphate buffers (Bai et al., 2015). For the present study, therefore, compositional properties and proton binding characteristics were compared among sub-fractions of FA. Specific objectives of this study are to: 1) describe compositions and principle components of sub-fractions of FA; 2) describe heterogeneity of binding sites for protons within sub-fractions by use of 2D-COS; 3) describe and compare values of p*K*a of fluorescent materials of sub-fractions.

2. Materials and methods

2.1. Sample pretreatment

Samples of surface soils used in this study were collected from Jiufeng Mountain forest, Beijing, China. After air-drying, soils were ground to pass through a 2 mm mesh. Soils were wetted with a dilute solution of HCl. Suspended solids were mixed and centrifuged to separate FA from the mineral fraction. The supernatant solution (solution A) was collected. The residue was neutralized with KOH by bubbling with nitrogen (N_2) gas and then centrifuged to obtain the supernatant. The supernatant solution was acidified with HCl and allowed to repeat the centrifugation. After centrifugation, the final liquid fraction (solution B) was collected and combined with solution A to obtain the entire FA solution. After purification using hydrogen fluoride, XAD-8 resin and H^+-saturated cation-exchange resin, FA was dissolved in pure water then loaded onto a column containing XAD-8 resin. XAD-8 resin coupled with pyrophosphate buffers with initial pH of 3.0, 5.0, 7.0, 9.0 and 13.0 were conducted to sequentially separate the purified FA into five sub-fractions, FA_3, FA_5, FA_7, FA_9, and FA_{13}, respectively. All sub-fractions of FA were re-purified and freeze dried (Bai et al., 2015; Song et al., 2017). Detailed information on isolation and fractionation of FA and its sub-fractions are described elsewhere (Bai et al., 2015).

2.2. Fluorescence titration

Sub-fractions of FA were diluted to equivalent concentrations of 10.0 mg/L, and ionic strength was adjusted to 0.05 mol/L $KClO_4$. Briefly, 100.0 mg of each sub-fraction of FA was dissolved in 100 mL water, and then filtered through 0.22 μm membrane. The mass of non-soluble sub-fraction of FA was calculated based on differences in mass of membrane and associated material. The filtered sub-fraction of FA was evaluated

according to the difference between weight of non-soluble sub-fraction and total weight, and then diluted with $KClO_4$ to 10.0 mg/L to be used as a stock solution. During titrations with acid and base values of pH were adjusted in 0.5 unit increments from 2.0 to 7.0 by addition of $HClO_4$ or KOH with different concentrations. To minimize hysteresis effects of the molecules of sub-fractions of FA, pH of each solution was equilibration time under nitrogen (N_2) for 15 min. To avoid static quenching caused by oxygen and buffering effects of carbonate species, fluorescence spectra were collected after stabilization of each pH during purging with N_2 for 15 min. In order to minimize effects of dilution, volumetric amounts of both $HClO_4$ and KOH solutions did not exceed 0.1% (*v*/v) of sub-fractions solutions (100 mL). Dilutions of FA sub-fractions and increases in ionic strength had no effects on fluorescence of FA sub-fractions during pH-dependent titration. All chemicals were analytical reagent grade unless otherwise noted. All solutions were prepared with Milli-Q water and filtered through 0.45 μm glass fiber filter membranes (Whatman, UK).

2.3. Fluorescence spectral analysis

Fluorescence spectra of sub-fractions were measured by use of a fluorescence spectrometer (Hitachi F-7000, Tokyo, Japan) with a 1 cm quartz cell. Slit widths were 5 and 10 nm for excitation (Ex) and emission (Em), respectively. Excitation wavelengths ranged from 200 to 550 nm with a constant wavelength offset of 30 nm. Scanning speed was 240 nm min^{-1}. Fluorescence of the $KClO_4$ blank was subtracted from SFS of sub-fractions and fluorescence intensities of SFS were presented in arbitrary units (a.u.). Peak wavelengths in SFS represented excitation values.

2.4. Principal component analysis

In this study, the PCA analysis of all 55 SFS sets (11 SFS data for each sub-fraction with pH in 0.5 unit increments from 2.0 to 7.0.) was performed by use of SPSS 16.0 software. PCs were extracted from the SFS data by PCA based on a complementary set of score and loading plots. Potential non-independence of the spectral data could influence the results of PCA, therefore, two parameters, Kaiser-Meyer-Olkin measure and Bartlett's test (*P*) of spectral data were used to test partial correlation and dependence (Guo et al., 2013).

2.5. Two-dimensional correlation analysis

2D COS was performed by use of 2D–Shige software derived by Kwansei Gakuin University (Tokyo, Japan). By extending the one-dimensional forms of variations into two-dimensional domains, 2D COS generated a synchronous map and an asynchronous map (Noda and Ozaki, 2009). Synchronous and asynchronous maps provided information about simultaneous and sequential changes of spectral intensity, respectively (Hur et al., 2011a; Noda and Ozaki, 2009). Spectral changes of $y(x,t)$, as a function of a spectral variable (x) and an external variable (t), and the dynamic spectra $\tilde{y}(x,t)$ can be represented (Eq. 1) (Hur et al., 2011; Noda and Ozaki, 2009).

$$\tilde{y}(x,t) = \begin{cases} y(x,t) - \bar{y}(x) & for\ T_{min} \le t \le T_{max} \\ 0 & otherwise \end{cases} \quad (1)$$

where, $\bar{y}(x) = \frac{1}{T_{max} - T_{min}} \int_{T_{min}}^{T_{max}} y(x,t)dt$ is the reference spectrum, denoting the t variable stationary or averaged spectrum.

The 2D synchronous spectrum is given by Eq. 2.

$$\varphi(x_1, x) = \frac{1}{T_{max} - T_{min}} \int_{T}^{T_{max}} \tilde{y}(x_1,t) \cdot \tilde{y}(x_2,t)dt \quad (2)$$

The 2D asynchronous spectrum can be obtained from the cross-correlation of the dynamic spectrum and the Hilbert-transformed orthogonal spectrum $z\sim(x_2,t)$ (Eq. 3).

$$\Psi(x_1, x_2) = \frac{1}{T_{max} - T_{min}} \int_{T}^{T_{max}} \tilde{y}(x_1,t) \cdot \tilde{z}(x_2,t)dt \quad (3)$$

In the synchronous maps, auto-peaks and cross-peaks can be observed at the main diagonal and the off-diagonal positions, respectively. In asynchronous maps, only cross-peaks appear at the off-diagonal positions (Chen et al., 2015; Noda, 1990; Noda and Ozaki, 2009). Under the influence of external forcing functions, the auto-peak represents the sensitivity of the correlation spectrum to changes in spectral intensity. In synchronous maps, cross-peaks represent the change of spectral intensity observed for two spectral variables ($v1$ and $v2$). Asynchronous cross-peaks show the sequential order of spectral variations induced by a perturbation. The sign of auto-peaks is always positive, while cross peaks can also be either positive or negative (Noda, 1990; Noda and Ozaki, 2009). If cross-peaks in both maps have the same sign in a given wavelength range, the spectral change at $v1$ precedes the change at $v2$. Otherwise, the reaction process is reversed according to Noda's rule (Chen et al., 2015; Noda, 1990; Noda and Ozaki, 2009). In this study, 2D COS was performed on 11 sets of SFS data for each sub-fraction of FA with the pH as the external perturbation. Additionally, 2D COS generated synchronous and asynchronous maps to provide detailed spectral variations of sub-fractions.

2.6. Determination of proton binding parameters

Fluorescence titration combined with use of the Stern-Volmer equation has been widely used for characterizing binding behaviors of DOM with metal ions (Esteves da Silva et al., 1998; Yamashita and Jaffé, 2008). In this study, dissociation constants (p*K*a) of sub-fractions were estimated by use of modified Stern-Volmer equation, based on data for wavelengths corresponding to main peaks in the synchronous-asynchronous maps derived from 2D COS. Reactions of proton binding of sub-fractions (represented by *L*) at pH 2.0–7.0 and the corresponding value of *K*a could be expressed (Eqs. 4 and 5).

$$HL \leftrightarrow L + H \quad (4)$$

$$Ka = \frac{[L][H]}{[HL]} \quad (5)$$

Where: [*HL*] is the equilibrium concentration of binding process; [*H*] is the equilibrium concentration of proton, which were not involved in the main reaction; [*L*] is the equilibrium concentration of ligands which were not involved in the main reaction.

In order to quantify p*K*a, it was assumed that FA molecules in sub-fractions had consistent fluorescence characteristics during fluorescence titration. Additionally, fluorescent binding sites in sub-fractions were also assumed to form 1:1 stoichiometry with protons. Fluorescence intensity, the total concentration of ligands (C_L) and the concentrations of [*HL*] were described (Eq. 6).

$$\frac{[HL]}{C_L} = \frac{F_0 - F}{F_0 - F_{end}} \quad (6)$$

Where: F and F_0 are the measured fluorescence intensities at certain pH and at the beginning of the proton fluorescence titration; F_{end} indicated fluorescence intensity at the end of titration. Based on the assumptions, the modified Stern-Volmer equation could be used in our study to estimate the values of p*K*a (Eqs. 7 and 8).

$$\frac{F_0 - F_{end}}{F - F_{end}} = \frac{[H]}{K_a} + 1 \quad (7)$$

Letting $f=\frac{(F_0-F_{end})}{F_0}$, the final relationship was derived:

$$\frac{F_0}{F_0-F}=\frac{F_0}{\Delta F}=\frac{K_a}{f[H]}+\frac{1}{f} \quad (8)$$

The parameters of f and Ka are the fraction of the initial fluorescence that corresponds to the binding fluorophores and the dissociation constant, respectively.

Fluorescence characteristics occurring in sub-fractions of FA might not be uniformly distributed among all components of sub-fractions, such that binding of protons might not be simply proportional to all binding sites in sub-fractions. The modified Stern-Volmer equation could not estimate the portion of unbound fluorescence contribution if stable non-fluorescent binding to proton were formed and/or if fluorescence data at a particular wavelength pair represents more than two binding sites. Despite these underlying limitations, the modified Stern-Volmer function was still useful for quantifying interactions between chemical species and DOM. Therefore, the SFS data were fitted by use of the modified Stern-Volmer equation with Origin 9.1 software.

3. Results and discussion

3.1. Synchronous fluorescence spectra

Three primary peaks, Peak A (272–280 nm), Peak B (328–368 nm) and Peak C (428–488 nm), were observed in SFS of FA_3–FA_{13} (Table 1, Fig. 1). The prominent presences of Peak A were distinguished in the SFS of FA_7–FA_{13} (Fig. 1). Unclear shoulders (~250 nm) observed in the SFS of both FA_3 and FA_5 were likely due to overlapping fluorescence of Peak A (Fig. 1). Previous studies had found that the common components in DOM, including protein-like (i.e., tyrosine-like and tryptophan-like materials), fulvic-like and humic-like materials, could be identified according to their SFS characteristics. The fulvic-like and humic-like materials had a higher degree of decomposition than both tyrosine-like and tryptophan-like materials, which are important constituents in the pool of aromatic amino acids (Bao et al., 2006; Chen et al., 2003; Heo et al., 2015; Zhou et al., 2013). Peak shoulders and Peaks A–C in SFS of sub-fractions of FA were located at fluorescence wavelength regions of tyrosine-like (250–265 nm), tryptophan-like (265–300 nm), fulvic-like (300–380 nm) and humic-like materials (380–550 nm), respectively (Table 1) (Chen et al., 2015; Esteves et al., 2006). Fluorescence intensities of Peak A (906–1906 a.u.) of FA_9 and FA_{13} were greater than those of FA_3–FA_7 (231–477 a.u.) at pH 7.0. Fluorescence intensity of Peak B (148 a.u.) of FA_3 was greater than those of Peak B (100–117 a.u.) of FA_5–FA_{13} at pH 7.0. Similarly, fluorescence intensity of Peak C (90 a.u.) of FA_3 was also greater than those of Peak C (33–51 a.u.) of FA_5–FA_{13} at pH 7.0 (Fig. 1). These results suggested that tryptophan-like materials were predominant in FA_9 and FA_{13}, and greater proportions of fulvic-like and humic-like materials were present in FA_3 at neutral pH. Fluorescence characteristics of sub-fractions of FA were pH-depended. This observation is consistent with previous reports (Pullin and Cabaniss, 1995). Those authors focused on effects of pH on SFS of the standard DOM reference material from the Suwannee River, USA offered by IHSS (Pullin and Cabaniss, 1995).

Table 1
Parameters of spectral peaks of sub-fractions of FA.

Peaks	Positions	Components
Peak A[a]	272–280 nm	Tryptophan-like materials
Peak B[a]	328–368 nm	Fulvic-like materials
Peak C[a]	428–488 nm	Humic-like materials
P1[b]	274 nm	Tryptophan-like materials
P2[b]	316 nm	Fulvic-like materials
P3[b]	428 nm	Humic-like materials
P4[b]	254 nm	Tyrosine-like materials
P5[b]	286 nm	Tryptophan-like materials
P6[b]	362 nm	Fulvic-like materials
P7[b]	454 nm	Humic-like materials

[a] The peak were observed from SFS in Fig. 1.
[b] The peak was observed from the plots of PCA factor scores vs. spectral wavelength in Fig. 2.

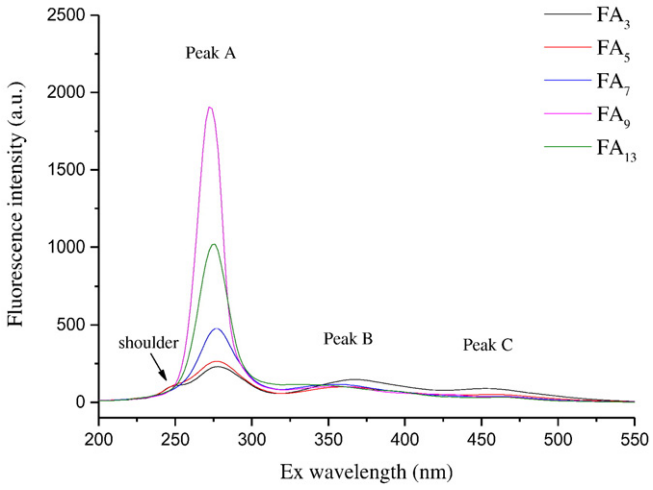

Fig. 1. SFS of sub-fractions of FA at pH 7.0.

3.2. Principal components analysis

Results of the Kaiser-Meyer-Olkin measure and Bartlett's test showed that all 55 SFS data of sub-fractions were suitable for PCA analysis with a smaller partial correlation between variables (0.95) and a larger dependence ($P < 0.001$). Two PCs (PC1 88.9% and PC2 8.8%) accounted for 97.6% of the total variance. To interpret SFS signals and identify fluorescent compounds of sub-fractions, plots of PCA factor scores versus wavelength were made (Fig. 2) (Guo et al., 2013; Hur et al., 2009; Su et al., 2016). From PC1 and PC2 plots, seven fluorescence peaks P1–P7 were centered at 274 nm, 316 nm, 428 nm, 254 nm, 286 nm, 362 nm, and 454 nm, respectively (Table 1, Fig. 2). The P1 and P5 were likely indicative of the presence of the tryptophan-like materials, which had similar locations within Peak A (Table 1, Figs. 1 and 2) (Guo et al., 2013). Peaks P2 and P6, which were in locations near to Peak B, were identified as fulvic-like materials (Table 1, Figs. 1 and 2) (Guo et al., 2013). Peaks P3 and P4 were attributable as humic-like materials, which had similar locations with Peak C (Table 1, Figs. 1 and 2) (Guo et al., 2013). A novel peak (P4) was identified by PCA analysis (Fig. 2b), which was related to tyrosine-like materials with shoulders at about 250 nm in SFS of FA_3 and FA_5 (Fig. 1). That is, PCA probably had an advantage to increase sensitivity and reduce spectroscopic overlap than was observed in original fluorescence spectra. The P5-P7 had 12 nm, 46 nm and 26 nm longer wavelengths than corresponding P1–P3, respectively (Table 1, Fig. 2). Previous studies have documented that DOM exhibiting longer excitation wavelengths, contained carbonyl, carboxyl, hydroxyl, alkoxyl constituents (Chen et al., 2002). The longer excitation wavelengths for P5-P7 might indicate that fluorescent components corresponding to PC2 had relatively large amounts of un-saturated π-π bonds and alkoxyl groups (Chen et al., 2002).

Four main clusters (Clusters I-IV) were identified from PCA factor loadings to establish a classification scheme for sub-fractions based on their different fluorescence signals at pH 2.0–7.0 (Table S1, Fig. 3). Cluster I including samples of FA_9 and FA_{13} at pH 2.0–7.0 exhibited a large loading to PC1 (>0.80) and a lesser loading to PC2 (<0.50) (Table S1, Fig. 3). On the contrary, Cluster IV including samples of FA_3 at pH 2.0–7.0 had a larger loading to PC2 (>0.85) and a lesser loading to PC1 (<0.50) (Table S1, Fig. 3). These results indicated a greater content of tryptophan-like materials in both FA_9 and FA_{13}, and greater proportion of fulvic-like materials in FA_3. Similar results were also obtained by

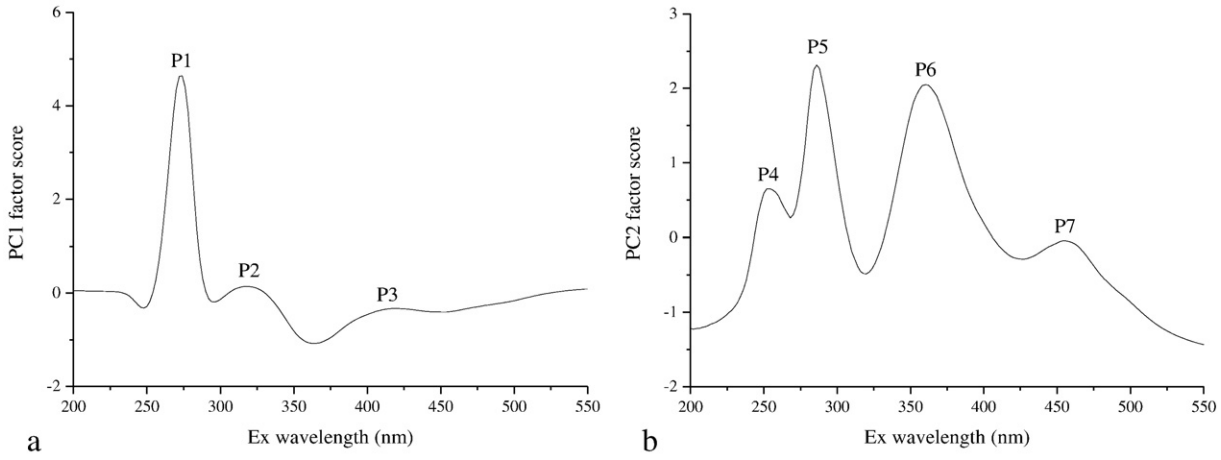

Fig. 2. PCA factor scores vs. spectral wavelength: PC1 (a); PC2 (b).

analysis of the fluorescence intensity of original SFS (Fig. 1) and the fluorescence excitation-emission matrix of sub-fractions of FA (Bai et al., 2015). Cluster II including samples of FA_7 at pH 5.5–7.0 obtained a relatively larger PC1 loading (>0.70). However, Cluster III including samples of FA_5 at pH 2.0–7.0 and FA_7 at pH 2.0–5.0 exhibited a relatively larger PC2 loading (>0.70) (Table S1, Fig. 3). Larger changes in loadings of the PCA appeared for FA_7 with pH 2.0–7.0, which might be due to comparable intensities of Peaks A-C (Figs. 1 and 3). Smaller changes of PC loadings were observed for FA_9 and FA_{13} with pH 2.0–7.0, which could be attributed to extra-strong intensities of Peak A compared to Peaks B and C (Figs. 1 and 3). Different changes in PC loadings as a function of pH suggested that proton binding sites might be unevenly distributed within the sub-fractions of FA.

3.3. Two-dimensional correlation fluorescence analysis

Synchronous and asynchronous maps derived from 2D-COS are shown for five sub-fractions of FA (Fig. 4). In the synchronous map, two main red/positive auto-peaks were observed for each sub-fraction in the range of FA_3–FA_7, and one main red/positive auto-peak was observed for each sub-fraction in the range of FA_9–FA_{13}. In synchronous and asynchronous maps, the cross-peaks must appear symmetrically along the diagonal line. Cross-peaks located at the bottom-left corner of synchronous and asynchronous maps were counted and analyzed. Therefore, one red/positive cross peak was present in the synchronous map of FA_3, and one blue/negative off-diagonal peak appeared for each synchronous map of FA_5 and FA_7 (Figs. 4 a1, c1). In asynchronous maps, cross peaks were observed at $v1$ wavelength ranges of 360–510 nm and narrow $v2$ wavelength ranges of 340–380 nm for FA_3. In contrast, cross peaks appeared at $v1$ wavelength ranges of 260–490 nm and narrow $v2$ wavelength ranges of 250–300 nm for FA_9 and FA_{13}. Cross peaks occupied both of the $v2$ narrow wavelength ranges of 250–300 nm and 350–400 nm in each asynchronous map for FA_5 and FA_7. The complicated distribution of peaks in synchronous and asynchronous maps for FA_3–FA_{13} might be related to heterogeneity of proton binding for different sub-fractions of FA. The heterogeneous distribution of binding sites of DOM had been reported previously (Hur and Lee, 2011a). Those authors focused on complexation of DOM and cupric ion by use of the 2D COS combined with fluorescence spectroscopy (Hur and Lee, 2011a).

In the synchronous map of FA_3, two main auto peaks (360/360 nm and 450/450 nm) were located at wavelength ranges of Peak B and

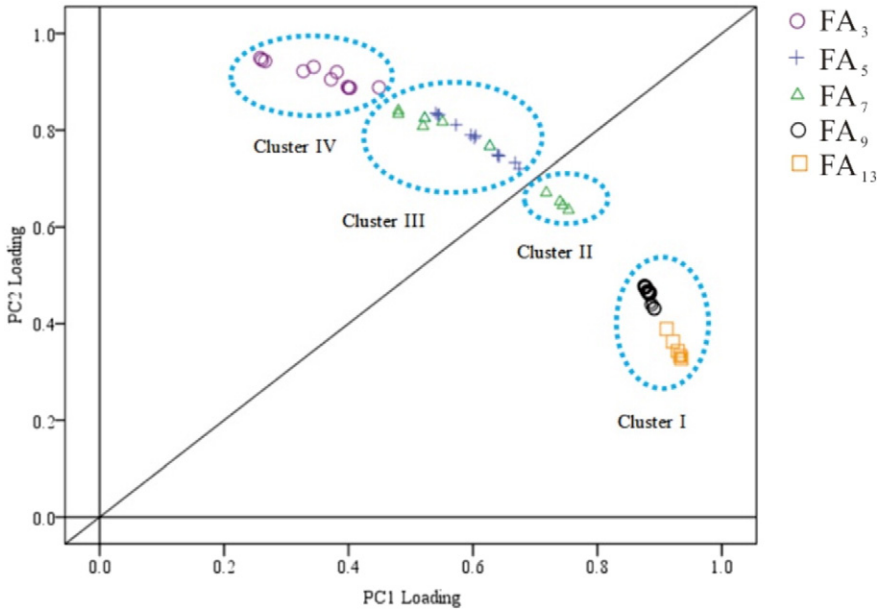

Fig. 3. SFS loading of sub-fractions on PC2 relative to PC1 at pH 2.0–7.0.

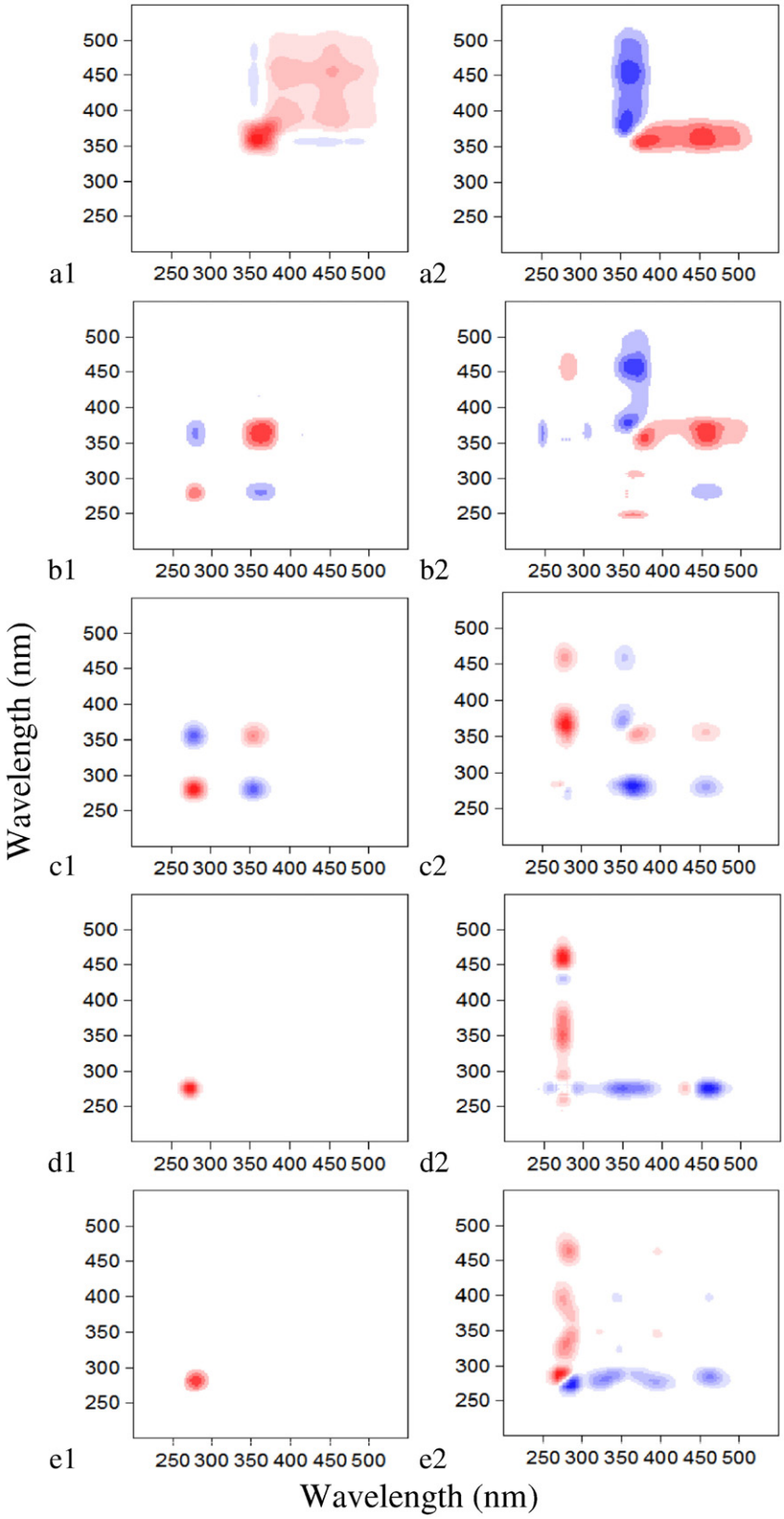

Fig. 4. 2D COS analysis of SFS sub-fractions of FA. Synchronous maps for FA_3–FA_{13} (a1–e1), asynchronous maps for FA_3–FA_{13} (a2–e2). The x-axis and y-axis are *v*1 and *v*2 respectively, derived by 2D-Shige software.

Peak C, respectively (Fig. 4 a1, Table 2). One main positive off-diagonal peak was observed near 450/374 nm (Fig. 4 a1, Table 2), which indicated that fulvic-like and humic-like materials occurred in the same direction with changing pH in FA_3. For each the synchronous maps of FA_5 and FA_7, two auto peaks were found near 274/274 nm and 360/360 nm along the diagonal line, which were associated with Peaks A and B, respectively (Fig. 4 b1, c1, Table 2). A cross peak with a negative sign located off the diagonal line at 360/274 nm was observed for synchronous

Table 2
2D COS results on the assignment and sign of peaks in synchronous and asynchronous (in the brackets) maps of sub-fractions of FA with proton binding.

Sub-fractions	Peak wavelength *v*1 (nm)	Assignment	Peak wavelength *v*2 (nm) and Signs					
			250	274	350	360	374	450
FA_3	360	Fulvic-like materials				+		
	374				(+)			
	450	Humic-like materials				(+)	−	+
FA_5	274	Tryptophan-like materials		+				
	360	Fulvic-like materials	(+)	−		+		
	374					(+)		
	450	Humic-like materials		(−)		(+)		
FA_7	274	Tryptophan-like materials		+				
	360	Fulvic-like materials		−/(−)	(+)	+		
	460	Humic-like materials		(−)	(+)			
FA_9	254	Tyrosine-like materials		(−)				
	274	Tryptophan-like materials		+				
	290			(−)				
	350	Fulvic-like materials		(−)				
	430	Humic-like materials		(+)				
	460			(−)				
FA_{13}	274	Tryptophan-like materials		+				
	290			(−)				
	324	Fulvic-like materials		(−)				
	374			(−)				
	460	Humic-like materials		(−)				

Note: Signs were obtained from synchronous and asynchronous maps. The + represents red/positive, − represents blue/negative.

maps of both FA_5 and FA_7 (Fig. 4 b1, c1, Table 2). This result indicated that, with changes of pH, changes in fulvic-like materials occur in a different direction than those of tryptophan-like materials. Detailed analyses showed that inconsistent changes in fluorescence intensities of fulvic-like materials as a function of pH, appeared for FA_5 and FA_7. This result was probably due to the influence of wavelength shift of a strong fluorescence peak around 290–390/340–520 nm (Song et al., 2017). For synchronous maps of FA_9 and FA_{13}, one positive auto-peak (274/274 nm) associated with Peak A was found along the diagonal line (Fig. 4 d1, e1, Table 2). This observation indicated that the spectral changes proceeded in the same direction with changing pH.

An asynchronous map revealed the degree of the sequential changes in two wavelengths as a function of changes of pH. In asynchronous spectra of the FA_3, two main positive peaks with wavelengths of 374/350 nm and 450/360 nm appeared below and off the diagonal line of the asynchronous map of FA_3 (Fig. 4 a2, Table 2). Based on Noda's rule, the degree of sequential changes followed the order of 374 nm → 350 nm, indicating that the heterogeneous distribution of proton binding sites even within a wavelength range (350–380 nm) associated with the same fluorescent materials (e.g., fulvic-like materials) for FA_3. In addition, the order of 450 nm → 360 nm for sequential changes suggested changes occurring in the order of humic-like → fulvic-like materials with changes of pH. This result indicated those sites to which protons bind in FA_3 were relatively homogeneously distributed over the wavelength range (360–450 nm) for fluorescent materials. Three main positive peaks (360/250 nm, 374/360 nm and 450/360 nm) and one weak negative peak (450/274 nm) were observed below and off the diagonal line in the asynchronous map of FA_5 (Fig. 4 b2, Table 2). Two negative peaks (360/274 nm and 460/274 nm) and two positive peaks (360/350 nm and 460/350 nm) were observed below and off the diagonal line in the asynchronous map of the FA_7 (Fig. 4 c2, Table 2). Therefore, the degree of sequential changes followed the order of 274 nm → 450 nm → 360 nm → 250 nm for FA_5 and 274 nm → 460 nm → 350 nm for FA_7. These results suggest that the order of variations of fluorescent materials was tryptophan-like → humic-like → fulvic-like → tyrosine-like materials for FA_5 and tryptophan-like → humic-like → fulvic-like materials for FA_7. Over the wavelength range of 250–460 nm, the heterogeneous distributions of proton binding sites for different fluorescent materials were also observed for FA_5 and FA_7. Four negative cross-peaks (254/274 nm, 290/274 nm, 350/274 nm and 460/274 nm) and one weak positive peak (430/274 nm) were observed in the asynchronous map of FA_9 (Fig. 4 d2, Table 2). In addition, four negative cross-peaks (290/274 nm, 324/274 nm, 374/274 nm and 460/274 nm) were observed in the asynchronous map of FA_{13} (Fig. 4 e2, Table 2). These results indicated that changes of fluorescence intensity occurring in tryptophan-like materials occurred prior to those occurring in tyrosine-like, fulvic-like and humic-like materials for FA_9 and fulvic-like and humic-like materials for FA_{13}. Furthermore, the degree of the sequential changes followed the order of 274 nm → 290 nm for both FA_9 and FA_{13} also suggested that the heterogeneous distribution of proton binding sites even within tryptophan-like materials for FA_9 and FA_{13}. Therefore, major advantage of using the SFS-PCA/2D-COS in this study would be to readily reduce extensive overlap of spectra and to capture subtle sequential differences in spectra over a range of wavelengths, providing a deep insight into protonation-dependent heterogeneity in fluorescent binding sites in sub-fractions of fulvic acid.

3.4. Proton binding parameters of FA sub-fractions

To quantitatively corroborate interpretations of 2D COS results, proton binding parameters were calculated by the fit of the modified Stern-Volmer equation at the wavelengths corresponding to the main positive or negative peaks in 2D COS maps (Table 3 and Fig. S1). In addition, the main positive and negative peaks occurring in 2D COS maps were also distinguished by use of PCA. The calculated values of p*K*a and *f* based on fluorescence properties ranged 2.20–5.29 and 0.10–0.54 for the sub-fractions of FA, respectively ($R > 0.894$) (Table 3). The values of p*K*a ranged of 2.20–3.38, 2.78–5.29, 2.39–4.15, 2.60–4.27 and 2.53–5.12 for FA_3–FA_{13}, respectively (Table 3). In general, values of p*K*a were comparable to those reported previous based on the properties of fluorescence excitation-emission matrix spectra (Midorikawa and Tanoue, 1998; Song et al., 2017; Wu and Tanoue, 2001).

Fluorescence peaks with wavelengths of 254–290 nm for FA_5–FA_{13} exhibited larger values of p*K*a (4.15–5.29) than those (2.20–3.38) of other peaks for sub-fractions of FA (Table 3). The presence of two adjacent aromatic carboxylic groups and/or an aromatic carboxylic group, and the adjacent phenolic group in sub-fractions of FA overwhelmingly contributed to changes in pH-dependent fluorescence (Midorikawa and Tanoue, 1998; Yan et al., 2013). Thus, protein-like materials of FA_5–FA_{13} might contain more aromatic structures and made stronger binding with protons. Different values of p*K*a of fluorescence peaks of sub-

Table 3
Proton binding parameters fitting by the modified Stern-Volmer equation.

Sub-fractions	Peak wavelength (nm)[a]	Modified Stern-Volmer equation		
		pKa	*f*	*R*
FA_3	350	2.20	0.43	0.985
	360	2.62	0.50	0.993
	374	2.54	0.51	0.990
	450	3.38	0.49	0.993
FA_5	274	5.29	0.14	0.894
	360	–	–	–
	374	–	–	–
	450	2.78	0.21	0.950
FA_7	274	4.15	0.37	0.996
	360	–	–	–
	460	2.39	0.40	0.997
FA_9	254	4.17	0.30	0.999
	274	4.27	0.54	0.999
	290	4.14	0.38	0.998
	350	–	–	–
	430	–	–	–
	460	2.60	0.30	0.984
FA_{13}	274	5.12	0.10	0.978
	290	4.57	0.16	0.986
	324	3.03	0.13	0.942
	374	2.76	0.23	0.909
	460	2.53	0.37	0.934

– data not available.
[a] The peak wavelengths were selected based on the plots of PCA factor scores vs. spectral wavelength in Fig. 2, and the synchronous and asynchronous maps of 2D COS in Fig. 4.

fractions were also a function of estimates of heterogeneity of binding sites of sub-fractions to protons (Table 3). This conclusion is consistent with that reported by Midorikawa and Tanoue (1998), who focused on oceanic DOM from North Pacific (Midorikawa and Tanoue, 1998).

Numbers of p*K*a values of selected peaks of sub-fractions of FA were reasonably consistent with previous interpretations of sequential orders determined by 2D COS analysis. As predicted from spectral features of the asynchronous maps and Noda's rules, decreasing trends of p*K*a values of peaks for FA_3 were observed in the order of 374 nm (2.54) → 350 nm (2.20) and 450 nm (3.38) → 360 nm (2.62). Values of p*K*a (4.15–5.29) of peaks located at 274 nm were greater than those (2.39–2.78) of peaks located at 450–460 nm for both FA_5 and FA_7, which were in agreement with results of the order of sequential changes with 274 nm → 360–460 nm in asynchronous maps of both FA_5 and FA_7. The p*K*a value of the peak at wavelength of 274 nm (4.27) for FA_9 was greater than those of other peaks at wavelengths of 254 nm (4.17) and 290–460 nm (2.60–4.14). Similarly, the p*K*a value of the peak at wavelength of 274 nm (5.12) for FA_{13} was greater than those of other peaks at wavelength range of 290–460 nm (2.53–4.57). These results are consistent with the interpretation of the corresponding spectral changes order in the asynchronous of FA_9 and FA_{13}. However, the p*K*a values of some selected peaks (e.g., 360 nm for FA_5 and FA_7) were not accurately established (Table 3), which might be attributed to the inconsistent changing direction and/or the smaller differences of fluorescence intensities with changes of pH (Song et al., 2017). The uncalculated stability constants of complexation between DOM and cupric ions were also reported base on the fluorescence peaks distinguished from 2D COS asynchronous maps (Hur and Lee, 2011a, 2011b).

4. Conclusion

Heterogeneous distributions of proton binding sites within sub-fractions of FA were identified by use of SFS-PCA/2D COS coupled with dissociation constants (p*K*a). Tryptophan-like, fulvic-like and humic-like materials were observed in SFS and the tyrosine-like materials were identified by use of SFS-PCA analysis. Relative differences of values of p*K*a within sub-fractions were consistent with the sequential orders derived from the asynchronous maps. In details, values of p*K*a derived from modified Stern-Volmer equation ranged from 2.20 to 5.29 for sub-fractions. Values of p*K*a of protein-like materials (4.15–5.29) were greater than those of sub-fractions of humic-like and fulvic-like materials (2.20–3.38). Variations occurred in order of humic-like → fulvic-like materials for FA_3, and both components changed in the same direction. Tryptophan-like materials in FA_5 and FA_7 had greater values of p*K*a (4.15–5.29) than humic-like, fulvic-like and tyrosine-like materials (2.39–2.78), which were consistent with the orders of variations of tryptophan-like → humic-like → fulvic-like → tyrosine-like materials for FA_5 and tryptophan-like → humic-like → fulvic-like materials for FA_7. Values of p*K*a of the tryptophan-like materials for each FA_9 (4.27) and FA_{13} (5.12) were greater followed by humic-like, fulvic-like and tyrosine-like materials, as expected for the higher variations of tryptophan-like materials from spectral patterns of the asynchronous maps of each FA_9 and FA_{13}. The binding sites heterogeneity for proton was also identified for single fulvic-like materials for FA_3 with the sequential changing order of 374 nm → 350 nm and the tryptophan-like materials for both FA_9 and FA_{13} with the order of 274 nm → 290 nm. The various binding sites can be readily recognized to elucidate the heterogeneous properties of DOM by use of SFS-PCA/2D COS combined with p*K*a, showing the great potential for further applications in revealing the interactions between DOM and environmental contaminants.

Acknowledgements

This work was financially supported by the National Natural Science Foundation of China (Nos. 41521003, 41630645, 41173084 and 41573130), Beijing Natural Science Foundation (8162044), Canada Research Chair program, Einstein Professor Program of the Chinese Academy of Sciences, and High Level Foreign Experts program (#GDT20143200016).

Appendix A. Supplementary data

Supplementary data to this article can be found online at https://doi.org/10.1016/j.scitotenv.2017.10.190.

References

Bai, Y., Wu, F., Xing, B., Meng, W., Shi, G., Ma, Y., Giesy, J.P., 2015. Isolation and characterization of Chinese standard fulvic acid sub-fractions separated from forest soil by stepwise elution with pyrophosphate buffer. Sci Rep 5, 8273.
Bao, Z., Sun, S., Li, J., Chen, X., Dong, S., Ma, H., 2006. Direct identification of tryptophan in a mixture of amino acids by the naked eye. Angew. Chem. Int. Ed. 45, 6723–6725.
Berkovic, A.M., García Einschlag, F.S., Gonzalez, M.C., Pis, D.R., Mártire, D.O., 2012. Evaluation of the Hg^{2+} binding potential of fulvic acids from fluorescence excitation-emission matrices. Photochem. Photobiol. Sci. 12, 384–392.
Cabaniss, S.E., 2002. Synchronous fluorescence spectra of metal-fulvic acid complexes. Environ. Sci. Technol. 26, 1133–1139.
Cabaniss, S.E., Shuman, M.S., 2002. Fluorescence quenching measurements of copper-fulvic acid binding. Anal. Chem. 60, 2418–2421.
Chen, J., Gu, B., Leboeuf, E.J., Pan, H., Dai, S., 2002. Spectroscopic characterization of the structural and functional properties of natural organic matter fractions. Chemosphere 48, 59–68.
Chen, W., Westerhoff, Paul, And, J.A.L., Booksh, K., 2003. Fluorescence excitation-emission matrix regional integration to quantify spectra for dissolved organic matter. Environ. Sci. Technol. 37, 5701–5710.
Chen, W., Habibul, N., Liu, X.Y., Sheng, G.P., Yu, H.Q., 2015. FTIR and synchronous fluorescence heterospectral two-dimensional correlation analyses on the binding characteristics of copper onto dissolved organic matter. Environ. Sci. Technol. 49, 2052–2058.
Chin, Y.P., Miller, P.L., Zeng, L., Cawley, K., Weavers, L.K., 2004. Photosensitized degradation of bisphenol a by dissolved organic matter. Environ. Sci. Technol. 38, 5888–5894.
De Haan, H., Werlemark, G., De Boer, T., 1983. Effect of pH on molecular weight and size of fulvic acids in drainage water from peaty grassland in NW Netherlands. Plant Soil 75, 63–73.
Esteves da Silva, J.C.G., Machado, A.A.S.C., Oliveira, C.J.S., Pinto, M.S.S.D.S., 1998. Fluorescence quenching of anthropogenic fulvic acids by cu(II), Fe(III) and UO_2^{2+}. Talanta 45, 1155–1165.
Esteves, d.S., Joaquim, C.G., Tauler, R., 2006. Multivariate curve resolution of synchronous fluorescence spectra matrices of fulvic acids obtained as a function of pH. Appl. Spectroscopy 60, 1315–1321.

Gauthier, T.D., Shane, E.C., Guerin, W.F., Seitz, W.R., Grant, C.L., 1986. Fluorescence quenching method for determining equilibrium constants for polycyclic aromatic hydrocarbons binding to dissolved humic materials. Environ. Sci. Technol. 20, 1162–1166.
Geng, C., Xi, B., Zhao, Y., Li, M., He, X.S., Wei, Z., 2010. Effect of pH and ionic strength on synchronous fluorescence spectra of dissolved organic matter in landfill leachate. J. Northeast. Agric. Univ. 170, 220–224.
Giesy, J.P., Alberts, J.J., 1982. Trace Metal Speciation: The Interaction of Metals with Organic Constituent of Surface Waters.
Giesy, J.P., Briese, L.A., 1980. Metal binding capacity of northern European surface waters for Cd, Cu, and Pb. Org. Geochem. 2, 57–67.
Giesy, J.P., Alberts, J.J., Evans, D.W., 2010. Conditional stability constants and binding capacities for copper (II) by dissolved organic carbon isolated from surface waters of the southeastern United States. Environ. Toxicol. Chem. 5, 139–154.
Guo, X.J., Yuan, D.H., Li, Q., Jiang, J.Y., Chen, F.X., Zhang, H., 2012. Spectroscopic techniques for quantitative characterization of Cu (II) and Hg (II) complexation by dissolved organic matter from lake sediment in arid and semi-arid region. Ecotox. Environ. Safe. 85, 144–150.
Guo, X.J., Yuan, D.H., Jiang, J.Y., Zhang, H., Deng, Y., 2013. Detection of dissolved organic matter in saline-alkali soils using synchronous fluorescence spectroscopy and principal component analysis. Spectrochim. Acta A Mol. Biomol. Spectrosc. 104, 280–286.
Hays, M.D., Ryan, D.K., Pennell, S., 2004. A modified multisite Stern-Volmer equation for the determination of conditional stability constants and ligand concentrations of soil fulvic acid with metal ions. Anal. Chem. 76, 848–854.
Heo, J., Yoon, Y., Kim, D.H., Lee, H., Lee, D., Her, N., 2015. A new fluorescence index with a fluorescence excitation-emission matrix for dissolved organic matter (DOM) characterization. Desalin. Water Treat. 57, 20270–20282.
Hur, J., Lee, B.M., 2011a. Characterization of binding site heterogeneity for copper within dissolved organic matter fractions using two-dimensional correlation fluorescence spectroscopy. Chemosphere 83, 1603–1611.
Hur, J., Lee, B.M., 2011b. Comparing the heterogeneity of copper-binding characteristics for two different-sized soil humic acid fractions using fluorescence quenching combined with 2D-COS. Sci. World J. 11, 1865–1876.
Hur, J., Lee, D.H., Shin, H.S., 2009. Comparison of the structural, spectroscopic and phenanthrene binding characteristics of humic acids from soils and lake sediments. Org. Geochem. 40, 1091–1099.
Hur, J., Jung, K.Y., Jung, Y.M., 2011. Characterization of spectral responses of humic substances upon UV irradiation using two-dimensional correlation spectroscopy. Water Res. 45, 2965–2974.
Iimura, Y., Ohtani, T., Chersich, S., Tani, M., Fujitake, N., 2012. Characterization of DAX-8 adsorbed soil fulvic acid fractions by various types of analyses. Soil Sci. Plant Nutr. 58, 404–415.
Lehmann, J., Kleber, M., 2015. The contentious nature of soil organic matter. Nature 528, 60–68.
Lochmueller, C.H., Saavedra, S.S., 1986. Conformational changes in a soil fulvic acid measured by time-dependent fluorescence depolarization. Anal. Chem. 58, 1978–1981.
Lu, X., Jaffe, R., 2001. Interaction between hg(II) and natural dissolved organic matter: a fluorescence spectroscopy based study. Water Res. 35, 1793–1803.
Lü, C., Chen, L., Yang, Z., Liu, X., Han, L., 2013. Visual recognition of fishmeal and meat and bone meal using temperature-dependent two-dimensional correlation near-infrared spectroscopy. Appl. Spectrosc. 67, 1390–1394.
Maqbool, T., Hur, J., 2016. Changes in fluorescent dissolved organic matter upon interaction with anionic surfactant as revealed by EEM-PARAFAC and two dimensional correlation spectroscopy. Chemosphere 161, 190–199.
Midorikawa, T., Tanoue, E., 1998. Molecular masses and chromophoric properties of dissolved organic ligands for copper(II) in oceanic water. Mar. Chem. 62, 219–239.
Noda, I., 1990. Two-dimensional infrared (2D IR) spectroscopy: theory and applications. Appl. Spectrosc. 44, 550–561.
Noda, I., Ozaki, Y., 2009. Chapter 4. Generalized two-dimensional correlation spectroscopy in practice.
Pace, M.L., Reche, I., Cole, J.J., Fernández-Barbero, A., Mazuecos, I.P., Prairie, Y.T., 2012. pH change induces shifts in the size and light absorption of dissolved organic matter. Biogeochemistry 108, 109–118.
Pullin, M.J., Cabaniss, S.E., 1995. Rank analysis of the pH-dependent synchronous fluorescence spectra of six standard humic substances. Environ. Sci. Technol. 29, 1460–1467.
Sakurai, K., Goto, Y., 2007. Principal component analysis of the pH-dependent conformational transitions of bovine β-lactoglobulin monitored by heteronuclear NMR. Proc. Natl. Acad. Sci. 104, 15346–15351.
Song, F., Wu, F., Guo, F., Wang, H., Feng, W., Zhou, M., Deng, Y., Bai, Y., Xing, B., Giesy, J.P., 2017. Interactions between stepwise-eluted sub-fractions of fulvic acids and protons revealed by fluorescence titration combined with EEM-PARAFAC. Sci. Total Environ. 605–606, 58–65.
Su, B.S., Qu, Z., He, X.S., Song, Y.H., Jia, L.M., 2016. Characterizing the compositional variation of dissolved organic matter over hydrophobicity and polarity using fluorescence spectra combined with principal component analysis and two-dimensional correlation technique. Environ. Sci. Pollut. Res. Int. 23, 9237–9244.
Wu, F., Tanoue, E., 2001. Isolation and partial characterization of dissolved copper-complexing ligands in streamwaters. Environ. Sci. Technol. 35, 3646–3652.
Wu, F., Cai, Y., Evans, D., Dillon, P., 2004. Complexation between Hg(II) and dissolved organic matter in stream waters: an application of fluorescence spectroscopy. Biogeochemistry 71, 339–351.
Xu, H., Yu, G., Yang, L., Jiang, H., 2013. Combination of two-dimensional correlation spectroscopy and parallel factor analysis to characterize the binding of heavy metals with DOM in lake sediments. J. Hazard. Mater. 263, 412–421.
Yamashita, Y., Jaffé, R., 2008. Characterizing the interactions between trace metals and dissolved organic matter using excitation-emission matrix and parallel factor analysis. Environ. Sci. Technol. 42, 7374–7379.
Yan, M., Fu, Q., Li, D., Gao, G., Wang, D., 2013. Study of the pH influence on the optical properties of dissolved organic matter using fluorescence excitation-emission matrix and parallel factor analysis. J. Lumin. 142, 103–109.
Zhou, J., Wang, J.J., Baudon, A., Chow, A.T., 2013. Improved fluorescence excitation-emission matrix regional integration to quantify spectra for fluorescent dissolved organic matter. J. Environ. Qual. 42, 925–930.

Supporting Information

Protonation-dependent heterogeneity in fluorescent binding sites in sub-fractions of fulvic acid using principle component analysis and two-dimensional correlation spectroscopy

Fanhao Song[a], Fengchang Wu[a], Baoshan Xing[b], Tingting Li[a], Weiying Feng[a], John P. Giesy[a,c], Wenjing Guo[a], Hao Wang[a], Shasha Liu[a], Yingchen Bai[a*]

[a]State Key Laboratory of Environmental Criteria and Risk Assessment, Chinese Research Academy of Environmental Sciences, Beijing, 100012, China

[b]Stockbridge School of Agriculture, University of Massachusetts, Amherst, MA, 01003, USA

[c]Department of Biomedical and Veterinary Biosciences and Toxicology Centre, University of Saskatchewan, Saskatoon, Saskatchewan, SK, S7N 5B3, Canada

Number of Pages (including this cover sheet): 4

Number of Figures: 1

[*]Corresponding author: Tel.: +86-10-84931804; Fax: +86-10-84931804.

E-mail: baiyc@craes.org.cn.

Supporting Information Captions

Fig. S1. The representative modified Stern-Volmer plots for Peak A (274 nm) of FA_3 (a, R^2=0.946) and FA_{13} (b, R^2=0.969) at pH 2.0-6.5, respectively.

Table S1. Distribution of clusters for sub-fractions at pH 2.0-7.0.

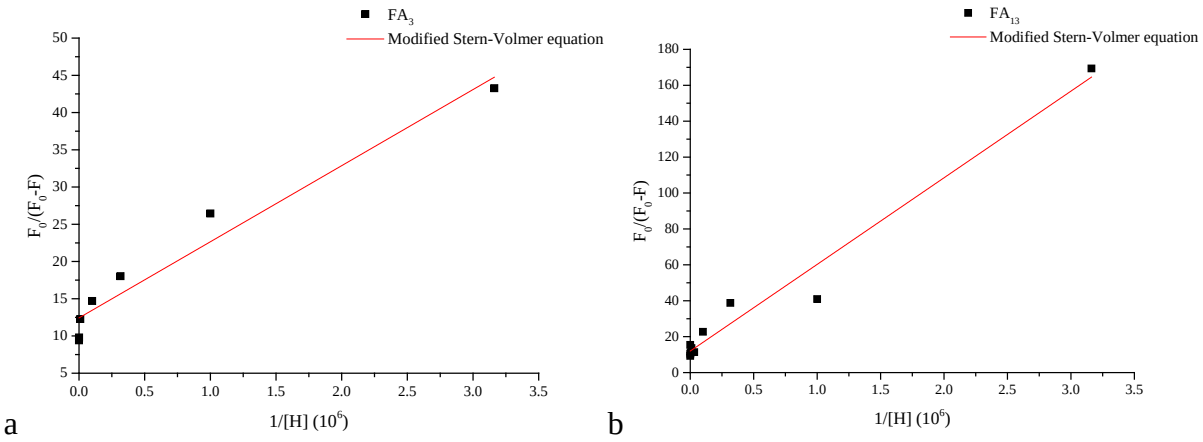

Fig. S1. The representative modified Stern-Volmer plots for Peak A (274 nm) of FA_3 (a, R^2=0.946) and FA_{13} (b, R^2=0.969) at pH 2.0-6.5, respectively.

Table S1. Distribution of clusters for sub-fractions at pH 2.0-7.0.

Clusters	PC1 loading	PC2 loading	Including samples
Cluster I	>0.80	<0.50	FA_9 (pH 2.0-7.0) and FA_{13} (pH 2.0-7.0)
Cluster II	<0.65	>0.70	FA_7 (pH 5.5-7.0)
Cluster III	>0.70	<0.70	FA_5 (pH 2.0-7.0) and FA_7 (pH 2.0-5.0)
Cluster IV	<0.50	>0.85	FA_3 (pH 2.0-7.0)